MODIFIED POINT-KINETICS MODEL FOR NEUTRON PRECURSORS AND FISSION PRODUCT BEHAVIOR FOR FLUID-FUELED MOLTEN SALT REACTORS[1]

M. Scott Greenwood and Ben Betzler

Oak Ridge National Laboratory

PO Box 2008, 1 Bethel Valley Road, Oak Ridge, TN 37831

greenwoodms@ornl.gov

betzlerbr@ornl.gov

Pages: 24

Tables: 8

Figures: 10

[1] Notice: This manuscript has been authored by UT-Battelle, LLC, under contract DE-AC05-00OR22725 with the US Department of Energy (DOE). The US government retains and the publisher, by accepting the article for publication, acknowledges that the US government retains a nonexclusive, paid-up, irrevocable, worldwide license to publish or reproduce the published form of this manuscript, or allow others to do so, for US government purposes. DOE will provide public access to these results of federally sponsored research in accordance with the DOE Public Access Plan (http://energy.gov/downloads/doe-public-access-plan).

ABSTRACT

Fluid-fueled nuclear reactors, such as molten salt reactors (MSRs), have recently gained significant interest. These advanced reactors represent a potential revolutionary shift in the implementation of nuclear power, and as a broad class of reactors, they have the potential to directly address many US energy policy objectives. Fuel which is dissolved in the coolant requires methods to account for the birth, decay, and transport of fission products not only in the core but throughout the loop and any auxiliary systems, such as off-gas, to which liquid fuel flows, gaseous products are carried, or solid particulates plate out. System models are particularly well suited to explore the wide range of phenomena which are associate with fluid-fueled systems, especially for safeguards analysis. However, before system dynamics can be explored the composition of fission products of the salt throughout the loop must be determined as they drive the dynamic behavior of a reactor.

This paper describes the derivation of a modified point kinetics model for obtaining a first-order approximation of the behavior of a salt-fueled system in which neutron precursors and fission products are born in the fuel-salt and transported outside the core. This paper also provides verification of the model using a steady-state analytic solution and provided additional cases exploring the response under transient cases. This model establishes a baseline model which can be used to explore the dynamic response of fluid-fueled reactors and investigate important safeguards issues such as mass-accountability of source terms. The model is implemented in the ORNL-developed, Modelica-based TRANSFORM library which was developed to investigate various aspects of advanced energy systems.

Key words: point kinetics, molten salt reactor, fission products

I. Introduction

The past few years have seen a significant increase in the interest of advanced fluid-fueled reactor systems, principally molten salt reactors (MSR). A fluid-fueled reactor is any reactor in which the fissile material is carried by the primary coolant throughout the primary flow circuit. Reactors such as MSRs represent a potential revolutionary shift in the implementation of nuclear power, and as a broad class of reactors, they have the potential to directly address many US energy policy objectives. One principal issue that arises when using a fluid-fueled reactor design is the production of delayed neutron precursors and other fission products in the core and subsequent transportation out of the core and the rest of the primary circuit and ultimate return to the core. Additional items of importance beyond just the fission product transport is the decay-chain, subsequent heat deposition, and even removal via auxiliary systems such as an off-gas system. The kinetic behavior of the reactor core in a fluid-fueled system, coupled with physical transport of source terms, requires a modified handling of traditional kinetic models such as the point kinetics model.

Proper accounting of radioactive source terms such as a neutron precursor or, more generally, a fission product location and concentration is key to successful licensing and safety evaluations, as these substances drive the performance of the reactor system under investigation. Accounting for source terms in traditional nuclear reactors such as light water reactors relies on fixed fuel forms such as cladded fuel. Assumptions regarding these traditional elements are reflected in the existing tools available to industry and regulators like the TRACE[1] code from the US Nuclear Regulatory Commission (NRC), which assumes that all source material is in a fixed location. Although modifications to the source code are possible depending on the use case[2,3], they are not officially endorsed, and if modifications are possible, it can take significant resources to implement them. Alternative, near-term, approaches to investigating the salt-fueled reactor systems enable the science to move forward and help define the requirements of advanced systems and the new, or modified/updated (e.g. TRACE), tools to develop and license them.

Additional methods of calculating the kinetic behavior of fluid-fueled systems have been summarized by Wooten and Powers[4]. Methods explored included variations of computationally expensive multi-group diffusion (MGD) methods, less expensive methods based on modified point reactor kinetics (PRK), quasi-static methods which are an attempt to bridge the attributes of MGD and PRK, and acceleration techniques using fission matrices. The authors conclude that each of these methods have merit, however those which couple directly with the thermo-hydraulics are most suitable for investigating the steady-state and transient behavior of a fluid-fueled system such as an MSR. Prior PRK methods have attempted to account for the delayed precursor movement with a variety of approaches including modifications to β_{eff}[5], *a-priori* knowledge of an initiating event to modify reactivity[6], and use of time constants to describe fission product behavior[7–9]. However, each of the reviewed methods do not approach species characterization from a mass accounting perspective. Rather, the models are applicable for short time intervals where isotopic composition were not considered. Evaluation of holistic systems behavior of fluid-fueled reactors, such as integration of off-gas systems and safeguards analysis, requires longer time-scales (i.e., isotopic changes) and knowledge of mass concentrations not only in the core but throughout the system. There exists a need to generate a flexible, physical quantity driven point kinetics model which can be integrated into a larger systems analysis to evaluate more complex dynamics of fluid-fueled systems.

This paper describes the derivation of a modified point kinetics model for obtaining a first-order approximation of the kinetic behavior of a salt-fueled system in which neutron precursors and fission products are born in the fuel-salt and transported outside the core, including decay-chain considerations, decay heat, and reactivity feedback effects. The proposed method focuses on generating a general mass accounting approach which can then be readily integrated into more complex system level models. This paper also provides verification of the model using a steady-state analytic solution and explores the response under transient cases. The model is implemented in the ORNL-developed, Modelica-based TRANSFORM library[10] which was developed to investigate various aspects of advanced energy systems.

I.A. Modelica and TRANSFORM

Modelica[11,12] is a nonproprietary, object-oriented, equation-based programming language used to conveniently model complex physical and cyber-physical systems (e.g., systems containing mechanical, electrical, electronic, hydraulic, thermal, and control components). A key advantage of Modelica is its separation of physical models and the solvers of the models. This separation enables rapid generation of complex physical systems and control design in a single language without requiring that the user have deep knowledge of numeric solvers, code generation, etc. This work used the commercial Modelica development environment Dymola 2018 FD01.[13]

The TRANsient Simulation Framework of Reconfigurable Models (TRANSFORM) is a Modelica-based simulation environment developed at ORNL.[10,14] The tool's primary purpose is to provide a common simulation environment and baseline modeling resources to facilitate rapid development of dynamic advanced reactor models. Critical elements of this effort include (1) definition of standardized, common interfaces between models and components, (2) development of a library of baseline component modules to be assembled into full plant models using available geometry, design, and thermal-hydraulic data, (3) definition of modeling conventions for model and component development, and (4) establishment of user interfaces and support tools to facilitate simulation development and analysis.[14–16] The TRANSFORM library has been successfully used for a variety of projects, including investigations into the performance of nuclear hybrid energy systems [17–20] and tritium transport.[21]

I.B. Trace Substances

The Modelica language allows for a class called a *connector,* which allows a set of variables to always be defined between the connection of two models (e.g., in a fluid system: pressure, mass flow rate, specific enthalpy of the fluid, mass fraction of each species in the fluid, and trace substance mass weighted fraction).

For transport purposes, the delayed neutron precursors and other fission products are modeled as trace substances. A trace substance is assumed to be in such small quantities that it has an insignificant impact on the mass of the system. The trace substances are tracked as unspecified mass weighted fractions of the

primary flow. This means that the trace substances flow as a homogenous part of the primary fluid but do not participate in the normal mass balance of the primary fluid, and the absolute units of the traced substances are inconsequential. For example, if the primary fluid flows at 1 kg/s and a trace substance's (C) mass weighted fraction is 100 atoms C/kg fluid, then the primary fluid mass balance assumes that there is 1 kg/s of primary fluid, and the trace substance mass has its own "mass" balance tracking the 100 atoms/s flowing through the system. This method allows for the mapping of small quantities of substances on traditional thermal-hydraulic processes as a first-order approximation, obviating the need to create complex media proprieties, pressure loss functions, etc. The behavior of the primary fluid is driven by its own mass, energy, and momentum balances.

An alternative method to using a trace substance approach would be to model each of the fission products as separate phases. This approach would permit more direct alteration of fluid properties, such as thermophysical properties, but adds additional complexities such as fluid media correlations that quantify these relationships and more complex mass, energy, and/or momentum equations. That type of approach permits a higher fidelity method of capturing phase behavior. Although possible, they are most appropriate for special applications such as a dissolved gas having approached its solubility limit.[22] The complexities and computational cost are excessive and not appropriate for a large set of substances where the principal behavior of the substances in the flow are in such small quantities as to have no significant impact on the principal fluid properties or fluid behavior.

II. Modified Point Kinetics for Neutron Precursor Drift

This section describes (1) the derivation of a modified point kinetics model used to account for nonstationary precursor groups and (2) conversion from the unitless form of the point kinetics model to a mass-based model as required for transport in the system. Two different approaches are presented that converge to the same solution (Eqs. (1) and (7) vs. Eqs. (13) and (14)). The two approaches, (1) neutron and mass balances, and (2) unitless point kinetics model, provides verification of the developed model. An analytical model of a simplified scenario for verification of the numerical solution is also presented.

II.A. Intuitive Point Kinetics Model Approach

The intuitive approach was coined by Ott and Neuhold in their textbook on reactor dynamics.[23] Their approach considers the balance equation approach to neutron economy: specifically, that the rate of change of a delayed neutron precursor group is equal to the production rate—a function of the power level—less the decay rate of the group plus the difference in precursors entering/leaving the system, as shown in Eq. (1):

$$\frac{dC_k(t)}{dt} = \frac{\bar{\nu}\beta_k}{w_f}P(t) - \lambda_k C_k(t) + \dot{C}_{k_{in}}(t) - \dot{C}_{k_{out}}(t) \tag{1}$$

where C_k is the number of precursor atoms per group k, t is time, $\bar{\nu}$ is the average number of neutrons released per fission, β_k is the fraction of fission neutrons associated with each precursor group, w_f is the usable energy released per fission, P is the power [W], λ_k is the decay rate [s^{-1}] of each precursor group, and $\dot{C_k}$ is the precursor atom flow rate [atom/s] in and out as determined by the fluid mass and momentum balances.

The power generation defined by the reactor kinetics is derived by starting from the solution to the rate of change of neutrons for the one-speed diffusion equation, including delayed neutrons. The result is shown in Eq. (2). The derivation can be found in Duderstadt and Hamilton, Chapter 6.I.B[24], with an additional term for the external source of neutrons.

$$\frac{dn(t)}{dt} = \frac{\rho(t) - \beta}{\Lambda}n(t) + \sum_k \lambda_k C_k(t) + S_{ext} \tag{2}$$

where the effective delayed neutron fraction, β, is the sum of the delayed neutron group of each precursor group (k) defined by Eq. (3).

$$\beta = \sum \beta_k \tag{3}$$

Substituting the relationship between power and neutrons from Eq. (4) into Eq. (2) yields Eq. (5), which is the power form of the kinetics model.

$$P(t) = w_f \nu \Sigma_f n(t) \tag{4}$$

$$\frac{dP(t)}{dt} = \frac{\rho(t) - \beta}{\Lambda}P(t) + w_f \nu \Sigma_f \sum_k \lambda_k C_k(t) + w_f \nu \Sigma_f S_{ext} \tag{5}$$

Eq. (6) is introduced to give Eq. (7), which is the preferred form of the equation, as it removes the additional parameters $\Sigma_f$and ν:

$$\Lambda = \frac{1}{\nu \bar{\nu} \Sigma_f} \tag{6}$$

$$\frac{dP(t)}{dt} = \frac{\rho(t) - \beta}{\Lambda} P(t) + \frac{w_f}{\Lambda \bar{\nu}} \sum_k \lambda_k C_k(t) + \frac{w_f}{\Lambda \bar{\nu}} S_{ext} \tag{7}$$

where n is the number of neutrons, ρ is the reactivity, Λ is the mean neutron generation time, ν is the average neutron speed, Σ_f is the macroscopic fission cross section, and S_{ext} is an external source of neutrons [n/s] for startup. All other variables are as previously defined.

II.B. Unitless Point Kinetics Model Modification Approach

The unitless forms of the power level and precursor concentration are shown in Eqs. (8) and (9). The derivation can be found in Ott and Neuhold.[23] Eq. (9) is modified from the original reference with the addition of the unitless precursor concentration flow contributions.

$$\frac{dp(t)}{dt} = \frac{\rho(t) - \beta}{\Lambda} p(t) + \sum_k \lambda_k \zeta_k(t) \tag{8}$$

$$\frac{d\zeta_k(t)}{dt} = \frac{\beta_k}{\Lambda} p(t) - \lambda_k \zeta_k(t) + \dot{\zeta}_{k_{k_{in}}}(t) - \dot{\zeta}_{k_{k_{out}}}(t) \tag{9}$$

Substitution of Eqs. (10–12) into Eqs. (8) and (9) yields the dimensional forms of the power level and precursor concentration in Eqs. (13) and (14). These are identical to the intuitive point kinetics derivation in Eqs. (1) and (7), where $S_{ext} = 0$:

$$S_0 = \bar{\nu} \Sigma_f \phi_0 = \bar{\nu} \Sigma_f \nu n_0 \tag{10}$$

$$\zeta_k(t) = \frac{1}{\Lambda} \xi_k(t) = \frac{1}{\Lambda} \frac{C_k(t)}{S_0} = \frac{1}{\Lambda \bar{\nu} \Sigma_f \nu n_0} C_k(t) \tag{11}$$

$$p(t) = \frac{P(t)}{P_0} = \frac{P(t)}{w_f \nu \Sigma_f n_0} \tag{12}$$

$$\frac{dP(t)}{dt} = \frac{\rho(t) - \beta}{\Lambda} P(t) + \frac{w_f}{\Lambda \bar{\nu}} \sum_k \lambda_k C_k(t) \tag{13}$$

$$\frac{dC_k(t)}{dt} = \frac{\bar{\nu} \beta_k}{w_f} P(t) - \lambda_k C_k(t) + \dot{C}_{k_{in}}(t) - \dot{C}_{k_{out}}(t) \tag{14}$$

where p is the dimensionless power level, and ζ_k is the precursor concentration of group k. All other variables are as previously defined.

II.C. Point Kinetics – Analytic Model

A steady-state analytic solution was derived from previous efforts to explicitly provide solutions for a one-dimensional delayed neutron precursor drift model.[25] The time-dependent one-dimensional precursor equation is shown in Eq. (15), where v_f is the space- and time-dependent velocity of the fluid.

$$\frac{\partial \zeta_k(z,t)}{\partial t} + v_f(z,t)\frac{\partial \zeta_k(z,t)}{\partial z} = -\lambda_k \zeta_k(z,t) + \frac{\beta_k(t)}{\Lambda(t)} p(z,t) \tag{15}$$

Applying the steady-state condition yields the simpler, ordinary differential Eq. (16), which can then be converted to units of concentration in Eq. (17).

$$v_f(z)\frac{\partial \zeta_k(z)}{\partial z} = -\lambda_k \zeta_k(z) + \frac{\beta_k}{\Lambda} p(z) \tag{16}$$

$$v_f(z)\frac{\partial C_k(z)}{\partial z} = -\lambda_k C_k(z) + \frac{\beta_k \bar{\nu}}{w_f} P(z) \tag{17}$$

Integration of Eq. (17) yields Eq. (18), where A is a constant, and V and Q are defined by Eqs. (19) and (20).

$$\lambda_k C_k(z) = \lambda_k e^{-V(z)} \int e^{V(z)} Q(z) dz + A\lambda_k e^{-V(z)} \tag{18}$$

$$V(z) = \int \frac{\lambda_k}{v_f(z)} dz \tag{19}$$

$$Q(z) = \frac{\beta_k \bar{\nu} P(z)}{w_f v_f(z)} \tag{20}$$

If simplified, Eq. (18) is analytically solvable. For example, the results presented in this paper assume constant velocity—$v(z) = v$—and they also assume that a given power profile, $P(z)$, in the core and outside the core (i.e., $L_{core} < z < L_{core} + L_{loop}$) is at zero power, as in $P(z) = 0$. This divides the problem into a set of two equations for the loop and the core with the boundary conditions providing the solution to the constant A. The boundary conditions are set so that the precursor concentrations are continuous at the core-loop interfaces, i.e., the precursor concentration injected into the core inlet is equal to the loop outlet and the core outlet concentration is equal to the loop inlet.

III. Adaptation of the Modified Kinetics Model for Fission Product Behavior

This section describes the modifications made to the kinetic precursor drift model derived in Section 2 to include the generation, decay, and reactivity feedback of fission products and a shape factor for fission power to integrate with discretized models.

III.A. Generation and Decay

The generation rate and decay of fission products is formulated based on the dimensional form of the power level, as illustrated in Eq. (7). The rate of generation of a fission product based on the power level is represented by a balance of the various source and sink terms, as shown in Eq. (21). The representation accounts for the various sources of direct fission events, the decay of individual species and the associated parent-daughter relationships due to a decay, the removal of species due to neutron absorption, and the transported species from the primary fluid carrier:

$$Generation = FissionSource - DecaySink + DecaySource - AbsorptionSink + InFlow - OutFlow$$

$$\frac{dC_i}{dt} = \frac{P}{w_f}\sum_k FS_k \sum_m FT_{k,m} FY_{i,k,m} - \lambda_i C_i + \sum_k \lambda_k C_k PM_{i,k} - \frac{P}{w_f \Sigma_f}\sigma_{a,i} N_i + \dot{C}_{i_{in}}(t) - \dot{C}_{i_{out}}(t) \quad (21)$$

where C_i is the number of atoms of fission product i, P is power level [W], w_f is the usable energy released per fission [J/fission], FS is an array of the fractional composition (sum=1) of the fission sources (e.g., ^{235}U and ^{239}Pu), FT is a matrix of fractions of fissions which come from each fission type (i.e., thermal and fast) per fissile source, FY is a matrix of the fission yield of each species per fissile source per fission type, λ is the fission product decay constant [s^{-1}], PM is the parent matrix which defines the parent-to-daughter yield per decay (i.e., sum of each column = 1 or 0), Σ_f is the macroscopic fission cross section, σ_a is the neutron absorption cross section [m^2], and N_i is the number density of fission product i [atoms/m^3].

III.B. Reactivity Feedback

The reactivity feedback of the fission products is accounted for by associating the absorption of neutrons from fission products as a negative reactivity contribution to the power equation, which is Eq. (7).

The derivation of the reactivity feedback is taken from a neutron balance approach. Adding an additional term to Eq. (2) which describes the rate of neutron removal as a function of the neutron flux (ϕ [n/m^2-s]) and the macroscopic absorption cross section of the fission products (Σ_a [m^{-1}]) yields Eq. (22), where V is the fluid volume [m^3].

$$\frac{dn(t)}{dt} = \frac{\rho(t)-\beta}{\Lambda} n(t) + \sum_k \lambda_k C_k(t) + S_{ext} - \Sigma_a \phi V \tag{22}$$

Substituting Eqs. (4), (6), (23), and (24) into Eq. (22) yields Eq. (25).

$$\phi(t) = vn(t)/V \tag{23}$$

$$\Sigma_a = \sigma_{a,i} N_i \tag{24}$$

$$\frac{dP(t)}{dt} = \frac{\rho(t)-\beta}{\Lambda} P(t) + \frac{w_f}{\Lambda \bar{v}} \sum_k \lambda_k C_k(t) + \frac{w_f}{\Lambda \bar{v}} S_{ext} - \Sigma_a v P(t) \tag{25}$$

Combining the absorption term with the reactivity using Λ, Eq. (6), and summing the contributions of each fission product yields the final form, Eq. (26), with the fission product source a reactivity contribution, Eq. (27), to the power equation.

$$\frac{dP(t)}{dt} = \frac{\rho(t)-\beta+\Delta\rho_{fp}}{\Lambda} P(t) + \frac{w_f}{\Lambda \bar{v}} \sum_k \lambda_k C_k(t) + \frac{w_f}{\Lambda \bar{v}} S_{ext} \tag{26}$$

$$\Delta\rho_{fp} = -\frac{1}{\bar{v}\Sigma_f} \sum_k \sigma_{a,k} N_k \tag{27}$$

Additional sources of reactivity are incorporated into the reactivity term as normal, such as fluid temperature feedback, Eq. (28), where α_T is the temperature feedback coefficient [K^{-1}], T is the fluid temperature [K], and T_{ref} is the nominal reference temperature [K] of each fluid.

$$\Delta\rho_T = \alpha_T (T - T_{ref}) \tag{28}$$

III.C. Decay Heat

With the implementation of fission product generation, the associated decay heat can then be addressed. The current implementation accounts for two types of energy deposition—*near field* and *far field*. These categories can be physically explained as beta decay energy which deposits in the immediate vicinity of the decay, or near field, and a gamma energy which is deposited at the location of the modeler's discretion, or far field. For example, in the core, the beta energies may be deposited in the fluid, and the gamma energy may be split between fluid and structural material.

Given the complexities of decay energy, the beta energy is a weighted average of the possible decay paths, and the gamma energy is the total decay energy released to go to ground state from the decaying species minus the weighted average beta energy. The decay heat from a near-field decay energy (i.e., beta decay, Q_β [W]) deposited in the fluid volume is then described by Eq. (29).

$$\mathrm{Q}_\beta = \sum_k w_{\beta k} \lambda_k C_k \tag{29}$$

A-priori knowledge of the location of far-field heat deposition (i.e., gamma decay, Q_γ [W]) for a model is unknown, so its designation is left to the modeler. However, Eq. (30) is a possible representation of how it may be accounted for by applying a weight (ψ) on the deposition location where the $sum(\psi) = 1$. w_β is the isotope-dependent energy of the near-field decay, and w_γ is the isotope-dependent energy of the far-field decay for each species. These decay energies are included throughout a model where appropriate (e.g., location of the decay).

$$\mathrm{Q}_\gamma = \sum_k \psi_k w_{\gamma k} \lambda_k C_k \tag{30}$$

III.D. Fission Shape Factor

Often the fluid and solid regions of reactor core models are discretized to gain insight as to the spatial impact of various physical phenomena such as heat transfer and fluid momentum equations. To incorporate this modified kinetic model into discretized models a shape factor was introduced (SF) with the property indicated in Eq. 31 where j is the number of discretized nodes.

$$1 = \sum SF_j \tag{31}$$

$$P_j = P \cdot SF_j \tag{32}$$

The shape factor is multiplied by the power determined by the power equation (Eq. 26) to yield the fission power per node. Additional dimensions (i.e., radial) could be incorporated via an extension of the demonstrated method.

A simple modification is then made to previously presented equations to account for spatial effects (i.e., fission product generation, reactivity feedback, etc.) of the fission shape factor. Additional feedbacks, such as temperature, should likely be weighted by a related shape factor as well but the weighting is left to the

user's discretion as it can be incorporated external to the kinetics model and may vary depending on the feedback.

The modified equation of precursor concentration, Eq. (14), to account for spatial effects is shown in Eq. (33).

$$\frac{dC_{k,j}}{dt} = \frac{\bar{\nu}\beta_k}{w_f} P \cdot SF_j - \lambda_k C_{k,j} + \dot{C}_{k,j_{in}} - \dot{C}_{k,j_{out}} \tag{33}$$

The modified equation of power, Eq. (26), to account for spatial effects is shown in Eq. (34).

$$\frac{dP}{dt} = \frac{\rho - \beta + \Delta\rho_{fp}}{\Lambda} P + \frac{w_f}{\Lambda\bar{\nu}} \sum_j \left(\sum_k \lambda_k C_{k,j} \right) + \frac{w_f}{\Lambda\bar{\nu}} S_{ext} \tag{34}$$

The modified equation of fission product concentration, Eq. (21), to account for spatial effects is shown in Eq. (35).

$$\frac{dC_{i,j}}{dt} = \frac{P \cdot SF_j}{w_f} \sum_k FS_k \sum_m FT_{k,m} FY_{i,k,m} - \lambda_i C_{i,j} + \sum_k \lambda_k C_{k,j} PM_{i,k} - \frac{P \cdot SF_j}{w_f \Sigma_f} \sigma_{a,i} N_{i,j} + \dot{C}_{i,j_{in}} - \dot{C}_{i,j_{out}} \tag{35}$$

The modified equation of reactivity, Eq. (27), to account for spatial effects is the sum of each spatial reactivity equation, Eq. (36), as shown in Eq. (37).

$$\Delta\rho_{fp_j} = -\frac{\mathrm{SF_j}}{\bar{\nu}\Sigma_f} \sum_k \sigma_{a,k} N_{k,j} \tag{36}$$

$$\Delta\rho_{fp} = \sum_j \Delta\rho_{fp_j} \tag{37}$$

The modified equation of near and far field decay heat, Eq. (29) and Eq. (30), to account for spatial effects is shown in Eq. (38) and Eq. (39).

$$\mathrm{Q_{\beta,j}} = \sum_k w_{\beta k} \lambda_k C_{k,j} \tag{38}$$

$$\mathrm{Q_{\gamma,j}} = \sum_k \psi_k w_{\gamma k} \lambda_k C_{k,j} \tag{39}$$

IV. Results

A two-fluid zone (core and loop) model was generated (Figure 1) to interrogate the behavior of the presented kinetics model. The Modelica model implements Eq. (33) for precursors, Eq. (35) for fission products, and Eqs. (34), (36), (37), and (28) for the power equation. The time derivative is handled by the selected Modelica solver. Dymola's commercial version of a DASSL[26] solver was chosen for this example.

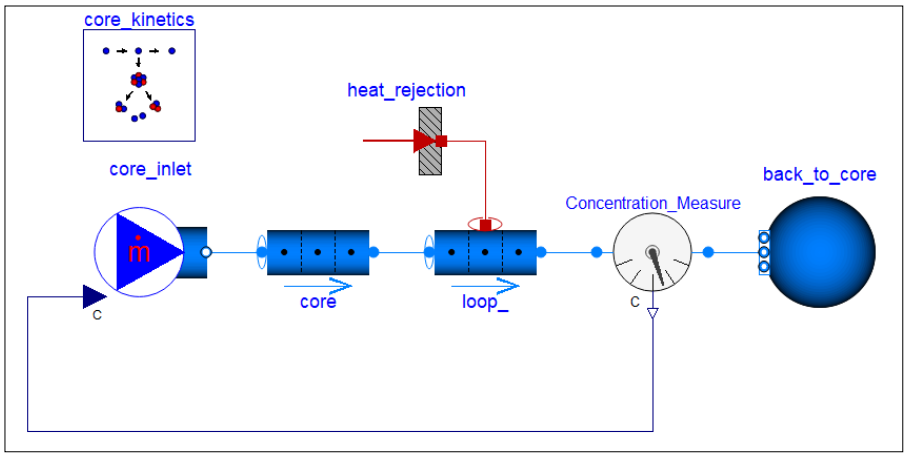

Figure 1: Simple TRANSFORM Modelica example of a closed-loop fluid model of a salt-fueled primary loop with a kinetic precursor drift model.

The implemented dynamic fluid model applies a fixed inlet mass flow rate and temperature at a variable pressure which satisfies the outlet boundary condition pressure. The inlet concentration of the neutron precursors and fission products are specified by the measured value at the outlet of the loop. No solid structures such as a pipe wall or moderating solid are included in this demonstration model. Heat transfer occurs only through the kinetic module in the core and through ideal heat rejection in the loop. Each zone of fluid is divided into nV distributed volumes which set the properties of the fluid. The base parameters of the model are summarized in Tables I–III where the neutron precursor data and loop specifications are taken from Betzler et al.[25] The fission product parameters for the simple case presented are taken from Chapter 6 of the reactor physics textbook by Stacey,[27] from the Chart of the Nuclides,[28] or they are set at arbitrary values for demonstration purposes.

Table I: Summary of the general parameters of the simulation.

Parameter	*Value*
nV_{core} [-]	10
nV_{loop} [-]	10
v_f [m/s]	0.4772
L_{core} [m]	3.4
L_{loop} [m]	6.296

Table II: Summary of the kinetic parameters of the simulation.

Parameter	*Value*
λ_k [s^{-1}]	0.0125, 0.0318, 0.109, 0.317, 1.35, 8.64
β [-]	0.0065
β_k x10^4 [-]	0.208, 1.082, 1.048, 2.987, 0.868, 0.307
$\bar{\nu}$ [-]	2.4
w_f [MeV]	200
Λ [s]	1e-5
α_T [K^{-1}]	-1e-4

Table III: Summary of the fission product parameters of the simulation.

Parameter	*Value*
FS [-]	1.0 (^{235}U)
FT [-]	1.0 (thermal)
FY [at/fis]	0.061, 0, 0.003
Σ_f [m^{-1}]	26
FP_i [-]	^{135}Te, ^{135}I, ^{135}Xe
FY [at/fis]	0.061, 0, 0.003
λ_i [s^{-1}]	0.036, 2.9e-5, 2.1e-5
σ_{a_i} [barns]	0, 0, 2.6e6
PM [yield/decay]	$\begin{bmatrix} 0 & 0 & 0 \\ 1 & 0 & 0 \\ 0 & 1 & 0 \end{bmatrix}$
w_β [MeV]	6000,1300,910
$\frac{w_{\beta,i}}{sum(w_\beta)}$ [-]	0.73, 0.16, 0.11
w_γ [keV]	603.5,1260.4,249.8
$\frac{w_{\gamma,i}}{sum(w_\gamma)}$ [-]	0.28, 0.60, 0.12
ψ [-]	1.0 (all in fluid)
S_{ext} [n/s]	0 (except Case 4 = 1)

Using the same base model, two steady-state cases (1 and 2) and two transient cases (3 and 4) were simulated from the summarized parameters. Cases 1 and 2 are direct comparisons to the analytical kinetics solution for verification of the neutron precursor kinetic drift model. For verification, Cases 3 and 4 are compared to simplified lumped models for fission product behavior presented in Eqs. (40) – (42). These equations are compared to the *total* atoms in the entire loop of the modified model.

$$\frac{dC_{Te}}{dt} = \frac{P}{w_f} FY_{Te} - \lambda_{Te} C_{Te} \tag{40}$$

$$\frac{dC_I}{dt} = \frac{P}{w_f} FY_I - \lambda_I C_I + \lambda_{Te} C_{Te} \tag{41}$$

$$\frac{dC_{Xe}}{dt} = \frac{P}{w_f} FY_{Xe} - \lambda_{Xe} C_{Xe} + \lambda_I C_I - \frac{P \cdot \sigma_{a,Xe} \quad C_{Xe} \quad L_{core}}{w_f \Sigma_f \quad CoreVolume L_{core} + L_{loop}} \tag{42}$$

where P is taken from the solution to the full model, C_* is the number of atoms of each fission product, and the remaining parameters are as defined previously. The ratio of of length of core to total length is required to account for the fraction of xenon not present in the core and therefore does not participate in the absorption reaction at any given time.

Fission product behavior is not included in Cases 1–2 to separate the exploration of the behavior. Cases 3 and 4 include the fission product behavior. Case 3 applies a fixed power input step from zero power (no power equation), and Case 4 implements a step reactivity input (e.g., simulated control rod ejection) from zero power using the power equation and reactivity feedback of fission products and temperature. These cases are summarized in Table IV.

Table IV: Case descriptions.

Case	*Description*
Assumptions for all cases	
	Fixed inlet mass flow rate and temperature
	Fixed outlet pressure
	Precursors and fission products core inlet concentration is equal to the loop outlet concentration
	Initial fluid temperature at 300°C
Steady-state neutron precursor cases	
1.	No power equation; fixed power $P(t) = P_0$ $SF = uniform$
2.	No power equation; fixed power $P(t) = P_0$ $SF = sinusoidal$
Transient fission product cases	
3.	No power equation; fixed, flat power step $P(t) = if\ time > 100\ or\ time < 0\ then\ P_0\ else\ 0$ $SF = uniform$
4.	Zero power initial with a flat reactivity step and temperature and fission product reactivity feedback $P_0 = 0$ $SF = sinusoidal$ $\rho(t) = \alpha_T(T_{fluid} - T_{ref}) + \rho_{Xe}$ $+ if\ time >$ $100\ or\ time < 0\ then - 1\ el$ $S_{ext} = 1$: needed since $P_0 = 0$

Normalized concentration is defined as the volume weighted concentration of species i divided by the maximum concentration of species i in the entire core and loop, Eq. (43) and Eq. (44).

$$Normalized\ Precursor\ Concentration = [C]_{i,j} = \frac{C_{i_j}/V_j}{\max\left(C_{i,:}/V_j\right)} \tag{43}$$

$$where\ j = 1{:}(nV_{core} + nV_{loop}) = 1{:}20 \tag{44}$$

Temperature is normalized by the reference temperature according to Eq. (45). All other parameters are normalized according by the maximum of the absolute value of the associated parameters.

$$T_{norm} = \frac{T - \min(T_{ref})}{\max(T_{ref}) - \min(T_{ref})} \tag{45}$$

Note, tables are given to provide scale for the normalized values presented in the figures. However, these values are highly dependent on the settings of the model and provide little value as the cases presented are simple demonstrations for exploring model dynamics. Regardless, they are provided for interested readers.

IV.A. Cases 1–2: Steady-State Neutron Precursor Behavior

The steady-state results of Cases 1 and 2 are shown in Figure 2 and Figure 3, respectively. The analytic method compares very well with the method implemented in Modelica. Irrespective of the case, the concentration (atoms of product per fluid mass in a constant volume) profile follows the expected behavior as the shorter a precursor groups half-life, the more it profile reflects the power shape of the case. Furthermore, upon leaving the core, the short half-life groups quickly decay to near zero while longer lived groups travel back to the core inlet in appreciable concentrations.

Although similar, some differences were expected between the analytical and numerical results as the analytic method is a much simpler problem than that solved with Modelica. The Modelica model has many other complex behaviors that affect aspects of the comparison, including temperature- and pressure-dependent fluid properties. However, these were accounted for where possible. Also, given the complexity of the Modelica model, the discretization of the fluid system must be coarse: in this example, $nV = 10$ nodes were used in the core, and 10 nodes were used in the loop. Increased nodalization would reduce the error between the analytical and Modelica models, but computational cost limits the number of nodes that

can be used in realistic scenarios to ~10 and is therefore presented. The maximum and minimum values of the normalized figures are given in Table V and VI.

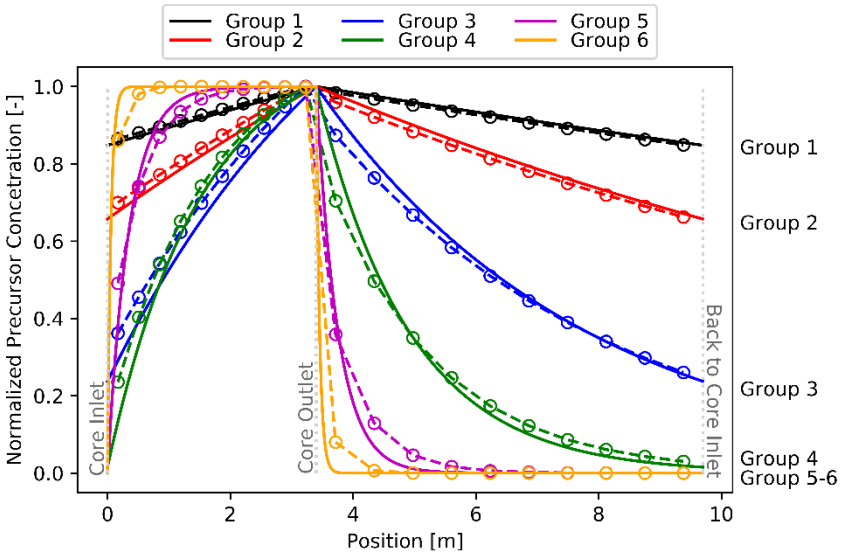

Figure 2: Case 1 normalized precursor concentration vs position (i.e., fixed, flat power profile); Modelica model = dashed circles; analytic model = solid lines.

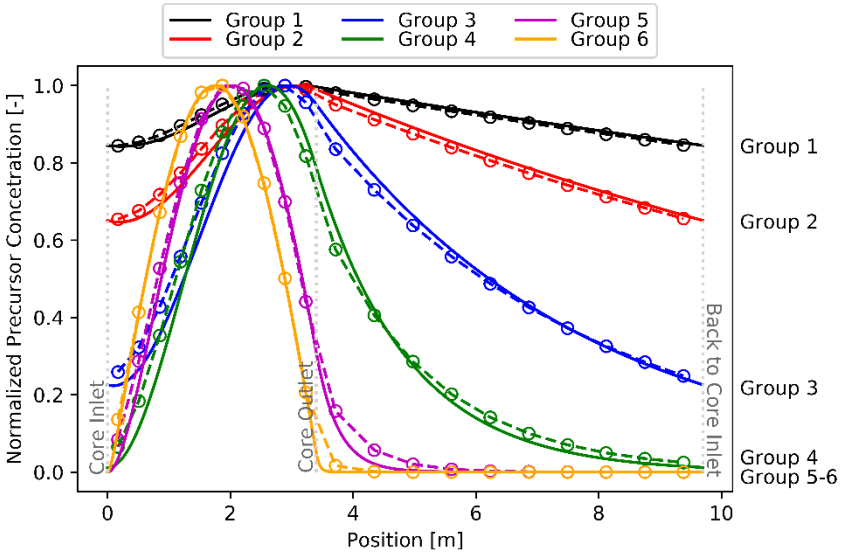

Figure 3: Case 2 normalized precursor concentration vs position (i.e., fixed, sinusoidal power profile); Modelica model = dashed circles; analytic model = solid lines.

Table V: Summary of maximum/minimum scaling for normalized Figure 2.

Parameter	*Maximum*	*Minimum*
Group 1 [atoms/kg]	3.33e13	2.83e13
Group 2 [atoms/kg]	7.64e13	5.06e13
Group 3 [atoms/kg]	3.04e13	7.92e12
Group 4 [atoms/kg]	4.33e13	1.31e12
Group 5 [atoms/kg]	3.38e12	1.21e8
Group 6 [atoms/kg]	1.87e11	2.14

Table VI: Summary of maximum/minimum scaling for normalized Figure 3.

Parameter	*Maximum*	*Minimum*
Group 1 [atoms/kg]	3.33e13	2.82e13
Group 2 [atoms/kg]	7.71e13	5.04e13
Group 3 [atoms/kg]	3.15e13	7.85e12
Group 4 [atoms/kg]	4.96e13	1.23e12
Group 5 [atoms/kg]	4.82e12	7.60e7
Group 6 [atoms/kg]	2.89e11	0.68

IV.B. Cases 3–4: Transient Fission Product Behavior

For each transient case, the plot takes the values from the last volume of the core for comparative purposes. Positional plots such as those used in Cases 1–2 are not as demonstrative due to the long half-lives of ^{135}Xe and ^{135}I as compared to the neutron precursor groups.

The transient case of a fixed power step from an initial zero power (Case 3) is shown in Figure 4 and Figure 5. This case demonstrates the proper response of the model with the expected bump in ^{135}Xe concentration following a rapid reactor shutdown from ^{135}I decay as the decay of each substance follows the exponential decay associated with their characteristic half-life. Furthermore, ^{135}Te closely follows the power step as expected due to its short half-life of 19 seconds. The maximum and minimum values of the normalized figures are given in Table VII.

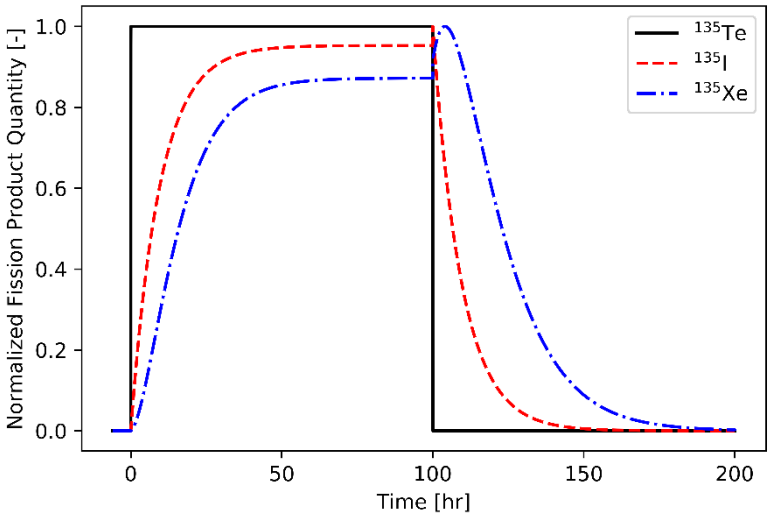

Figure 4: Case 3 fission product behavior for a fixed power step.

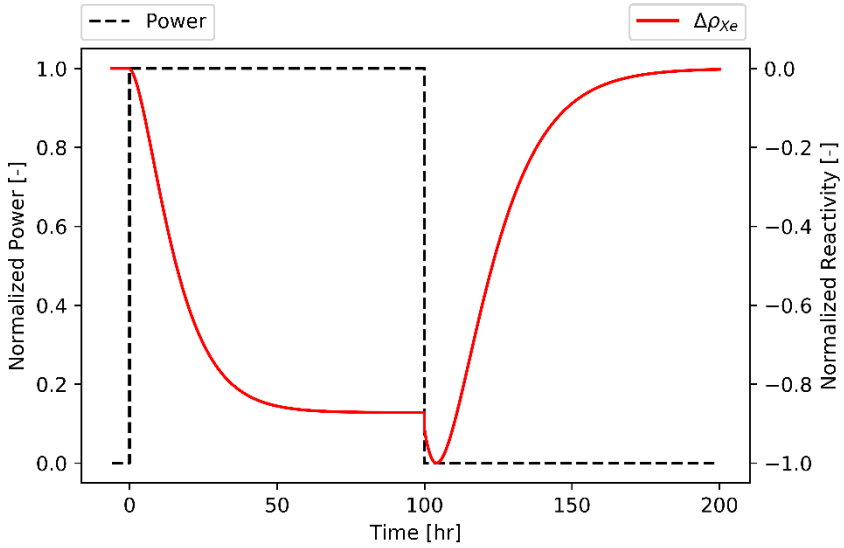

Figure 5: Case 3 normalized power and ^{135}Xe reactivity feedback. Feedback is shown for demonstrative purposes and has no direct feedback to the power level in Case 3 as the case sets the power output.

Table VII: Summary of maximum/minimum scaling for normalized Figures 4 – 5.

Parameter	*Maximum*	*Minimum*
^{135}Te [atoms]	1.14e15	0
^{135}I [atoms]	1.20e18	0
^{135}Xe [atoms]	1.08e18	0
$\Delta\rho_{Xe}$ [pcm]	0	-1286
Power [kW]	500	0

Figure 6 presents the comparison of the modified kinetic model to the simplified lumped model. As shown in the figure, there is very favorable comparison between the results which helps verify (e.g., time

constants and steady-state quantities) the more complex modified model. The small deviation of the modified model at the transient condition around 100 hours is associated abrupt temperature changes in the loop which change the density and therefore the mass of the fluid in each control volume.

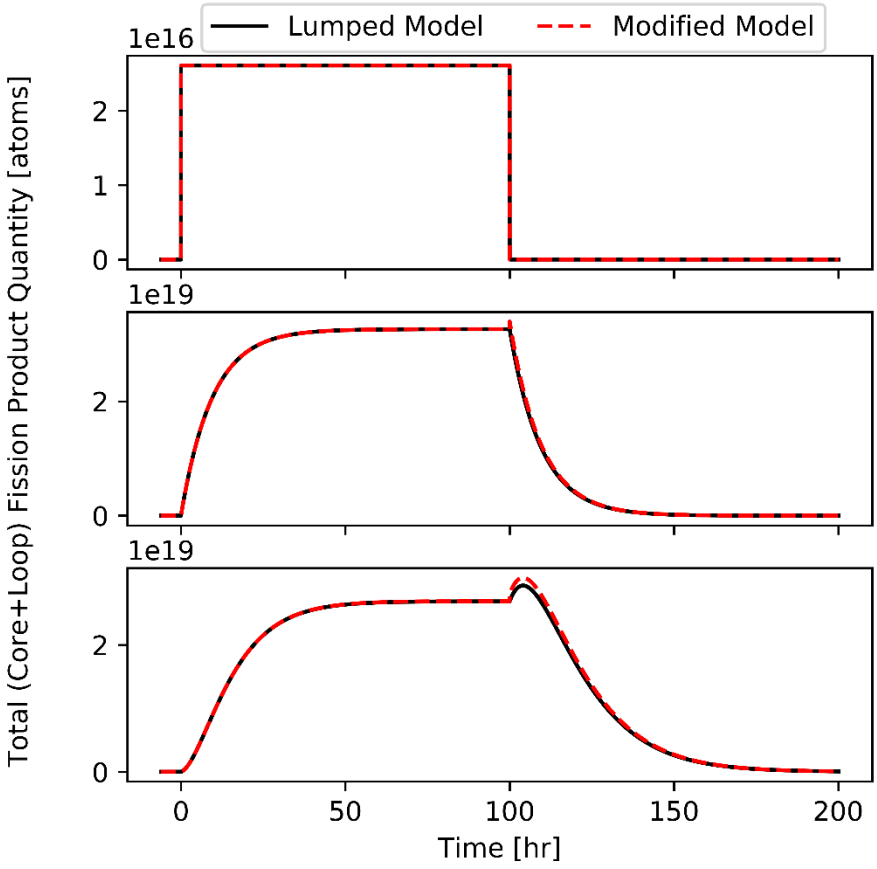

Figure 6: Case 3 comparison of the modified model to the simplified lumped model.

The results of a fixed reactivity insertion step from an initial zero power state (Case 4) are presented in Figure 7 through

Figure 10. The reactivity step for Case 4 (ρ_{CR} – Figure 8) is initially negative to achieve a zero-power condition. At time zero ρ_{CR} is stepped to zero. The fission product inventory builds up according to the power response of the system until a steady state condition is achieved. When the reactivity step ends, and a strong negative reactivity is reintroduced to the simulation, the products appropriately decay, while ^{135}Xe once again has the characteristic bump due to ^{135}I decay (Figure 7). Figure 9 verifies that the presented steady-state quantities and time constants are being calculated correctly.

The initial 300°C temperature of the fluid compared to the assumed sigmoidal reference temperature causes a large increase in the power of the reactor as the kinetics strive to correct the imbalance. As the temperature of the core rises to the reference state, the temperature quickly drops and then slowly rises again (see $\Delta\rho_T$) as the ^{135}Xe builds up in the system ($\Delta\rho_{Xe}$) until steady state is achieved (Figure 8). The *Power* variable has the shape of the total reactivity, which is the sum of the plotted reactivities, between the hours of 0 and 100 though not apparent on the figure due to the scale the change in reactivity. Upon shutdown, the fission products decay as before, and the power of the reactor quickly shuts down. However, the power of the reactor does not drop to zero, but rather to the level of the decay heat from the fission products (

Figure 10). In this case, the decay heat is very small compared to the steady-state levels, because not all primary fission product decay heat sources have been included and are therefore masked by the scale of the power change. $\Delta\rho_T$ returns to a maximum value of 1.0 when the reactor shuts down as the temperature of the core returns quickly returns to the boundary condition inlet temperature which is the minimum temperature encountered in this transient (i.e., the maximum reactivity difference). The near-field (β) decay power closely follows the initial rapid response of ^{135}Te due to its large β decay energy, while the far-field (γ) more closely corresponds to the slower γ decay of ^{135}I (Table III). The maximum and minimum values of the normalized figures are given in Table VIII.

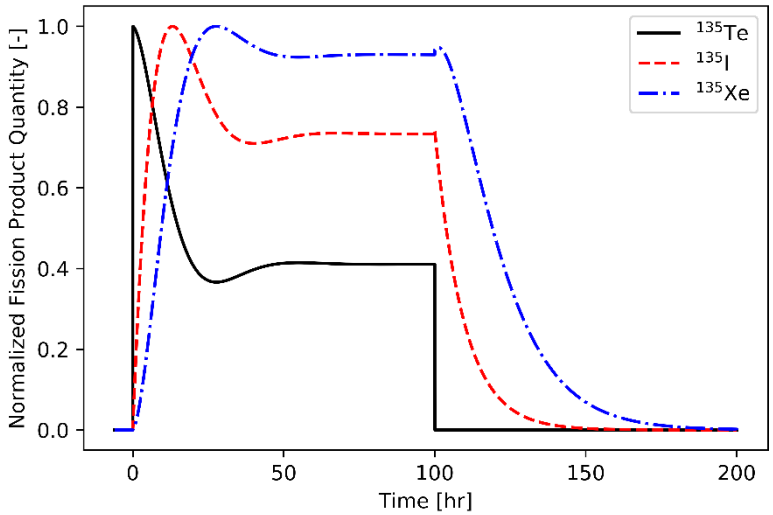

Figure 7: Case 4 fission product behavior for a fixed reactivity step from an initial zero power level.

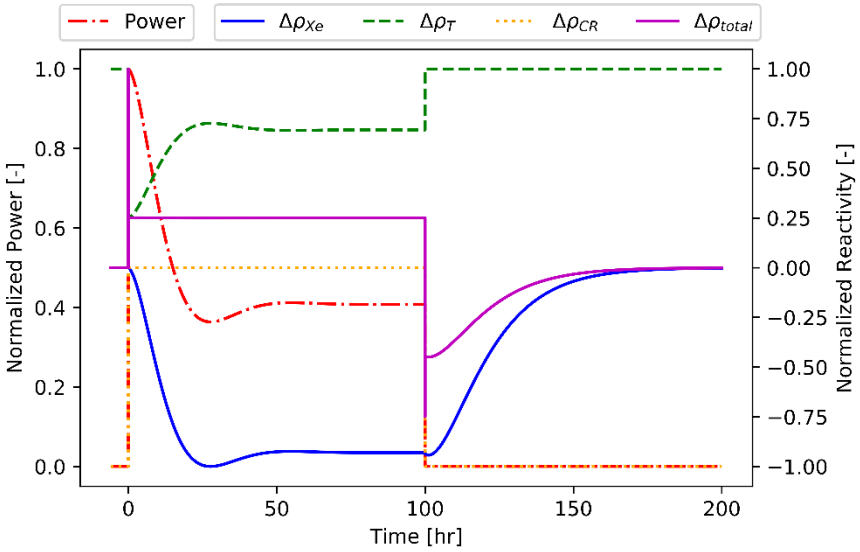

Figure 8: Case 4 normalized power, reactivity feedback (^{135}Xe and temperature), and controlled reactivity step.

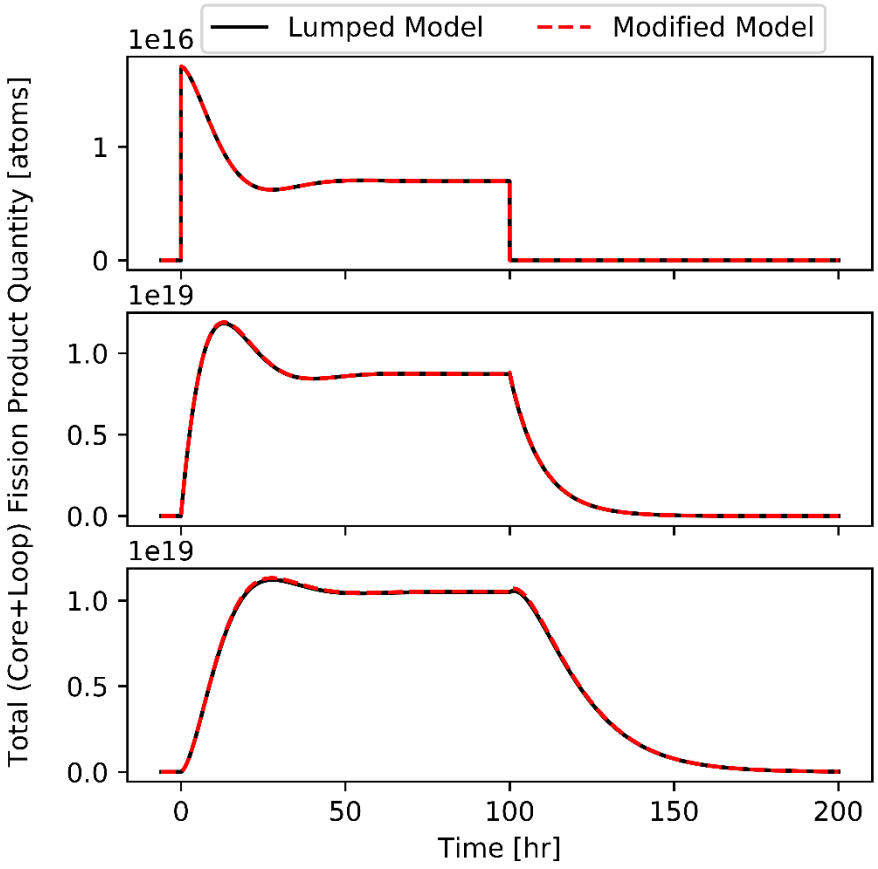

Figure 9: Case 4 comparison of the modified model to the simplified lumped model.

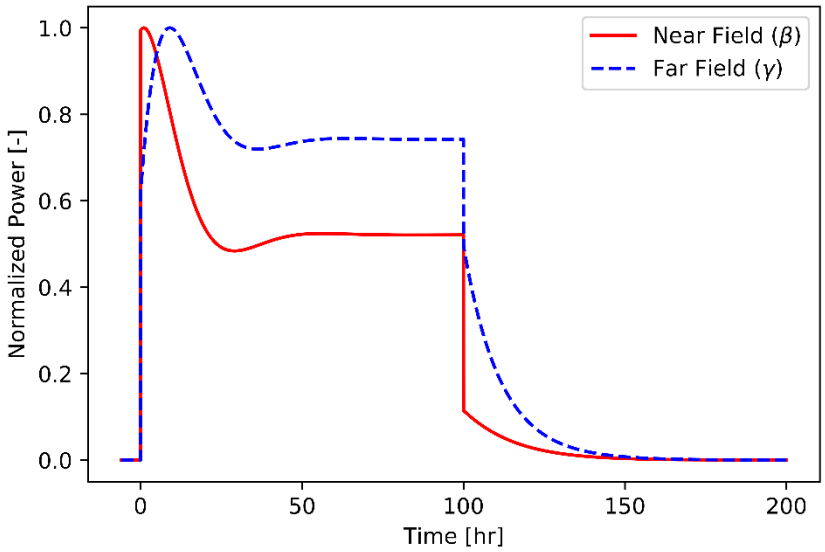

Figure 10: Case 4 decay heat from fission products (β and γ).

Table VIII: Summary of maximum/minimum scaling for normalized Figures 7, 8, and 10.

Parameter	*Maximum*	*Minimum*
^{135}Te [atoms]	7.52e14	0
^{135}I [atoms]	4.19e17	0
^{135}Xe [atoms]	3.98e17	0
$\Delta\rho_T$ [pcm]	1000	252
$\Delta\rho_{Xe}$ [pcm]	0	-477
$\Delta\rho_{CR}$ [pcm]	0	-1000
$Power$ [kW]	328	0
$Near\ Field\ (\beta)$ [W]	26.5	0
$Far\ Field\ (\gamma)$ [W]	4.33	0

V. Conclusion

A kinetic precursor drift model has been implemented in the ORNL Modelica-based TRANSFORM library for first-order investigations into the behavior of fluid-fueled molten salt systems using a trace substances approach. The model captures the creation, decay, and transport of precursor neutron groups and fission products, including decay heat in terms of near- and far-field energy deposition associated with the decay of fission products. The developed model has been successfully verified against an analytic solution of a simplified problem and demonstrated to reproduce reasonable behaviors for a variety of cases using an example which includes thermal-hydraulics, power generation, and reactivity feedback. The developed model will form the preliminary kinetics basis of additional investigations of more complex system-level behavior of fluid-fueled molten salt systems and comparisons to experimental data

VI. Acknowledgment

The authors would like to thank the US Department of Energy Office of Nuclear Energy Advanced Reactor Technology Molten Salt Reactor Campaign for funding this work.

VII. REFERENCES

1. NUCLEAR REGULATORY COMMISSION, “TRACE V5.0 Theory Manual: Field Equations, Solution Methods, and Physical Models,” US NRC.
2. X. HE, “Validation of the TRACE Code for the System Dynamic Simulations of the Molten Salt Reactor Experiment and the Preliminary Study on the Dual Fluid Molten Salt Reactor,” Technical University of Munich (2016).
3. P. AVIGNI, A. J. WYSOCKI, and G. L. YODER, “Liquid Salt Test Loop modeling using TRACE,” Ann. Nucl. Energy **106**, 170 (2017); https://doi.org/10.1016/j.anucene.2017.04.003.

4. D. WOOTEN and J. J. POWERS, “A Review of Molten Salt Reactor Kinetics Models,” Nucl. Sci. Eng. (In press).
5. D. ZHANG, A. RINEISKI, and Q. SUIZHENG, “Comparison of modeling options for delayed neutron precursor movement in a molten salt reactor,” in Transactions of the American Nuclear Society **100**, p. 639 (2009).
6. E. MERLE-LUCOTTE et al., “Physical assessment of the load-following and starting procedures for the Molten Salt Fast Reactor,” in Proceedings of ICAPP 2015, pp. 901–909 (2015).
7. N. SUZUKI and Y. SHIMAZU, “Reactivity-Initiated-Accident Analysis without Scram of a Molten Salt Reactor,” J. Nucl. Sci. Technol. **45** 6, 575 (2008); https://doi.org/10.1080/18811248.2008.9711881.
8. V. SINGH et al., “Dynamics and control of molten-salt breeder reactor,” Nucl. Eng. Technol. **49** 5, 887 (2017); https://doi.org/10.1016/j.net.2017.06.003.
9. V. SINGH et al., “Nonlinear dynamic model of Molten-Salt Reactor Experiment – Validation and operational analysis,” Ann. Nucl. Energy **113**, 177 (2018); https://doi.org/10.1016/j.anucene.2017.10.047.
10. M. S. GREENWOOD, *TRANSFORM - TRANsient Simulation Framework of Reconfigurable Models*, Modelica, Oak Ridge National Laboratory (2017); https://doi.org/10.11578/dc.20171109.1.
11. MODELICA ASSOCIATION, “Modelica and the Modelica Association;” https://www.modelica.org/; (current as of Aug. 16, 2017).
12. MODELICA ASSOCIATION, “Modelica Language Specification Version 3.4,” Modelica Association (2017).
13. DASSAULT SYSTEMES, “Dymola Systems Engineering;” https://www.3ds.com/products-services/catia/products/dymola/; (current as of Aug. 16, 2017).
14. R. HALE et al., “Update on ORNL TRANSFORM Tool: Preliminary Architecture/Modules for High-Temperature Gas-Cooled Reactor Concepts and Update on ALMR Control,” ORNL/SPR--2015/367, Oak Ridge National Laboratory (ORNL), Oak Ridge, TN (United States) (2015).
15. R. E. HALE et al., “Update on ORNL Transform Tool: Simulating Multi-Module Advanced Reactor with End-to-End I&C,” ORNL/SPR-2015/257, Oak Ridge National Laboratory (ORNL), Oak Ridge, TN (United States) (2015); https://doi.org/10.2172/1239756.
16. R. E. HALE et al., “Update on Small Modular Reactors Dynamic System Modeling Tool: Web Application,” ORNL/SPR--2015/17, Oak Ridge National Laboratory (ORNL), Oak Ridge, TN (United States) (2015); https://doi.org/10.2172/1252137.
17. M. S. GREENWOOD, “Component Development for Nuclear Hybrid Energy Systems,” presented at 12th International Modelica Conference, 7 May 2017, Prague, Czech Republic, 839–846; https://doi.org/10.3384/ecp17132839.
18. M. S. GREENWOOD, D. W. FUGATE, and S. M. CETINER, “Control Systems for a Dynamic Multi-Physics Model of a Nuclear Hybrid Energy System,” presented at 10th International Topical Meeting on Nuclear Plant Instrumentation, Control, and Human-Machine Interface Technologies, 11 June 2017, San Francisco, CA (United States).
19. C. RABITI et al., “Status Report on Modelling and Simulation Capabilities for Nuclear-Renewable Hybrid Energy Systems,” NL/EXT-17-42441, Idaho National Laboratory (2017).
20. M. S. GREENWOOD et al., “A Templated Approach for Multi-Physics Modeling of Hybrid Energy Systems in Modelica,” ORNL/TM-2018/757, Oak Ridge National Lab. (ORNL), Oak Ridge, TN (United States) (2017).
21. J. D. RADER, M. S. GREENWOOD, and P. W. HUMRICKHOUSE, “Verification of Modelica-Based Models with Analytical Solutions for Tritium Diffusion,” Nucl. Technol., 1 (2018); https://doi.org/10.1080/00295450.2018.1431505.
22. B. S. COLLINS et al., “Multiphysics Simulations of Molten Salt Reactors,” presented at Scale Workshop, 27 August 2018.
23. K. O. OTT and R. J. NEUHOLD, *Introductory Nuclear Reactor Dynamics*, American Nuclear Society, La Grange Park, Ill. USA (1985).

24. J. J. DUDERSTADT and L. J. HAMILTON, *Nuclear Reactor Analysis*, Wiley, New York (1976).
25. B. R. BETZLER et al., "Implementation of Molten Salt Reactor Tools in SCALE," presented at International Conference on Mathematics & Computational Methods Applied to Nuclear Science & Engineering, 16 January 2017, Jeju, Korea.
26. L. R. PETZOLD, "A Description of DASSL: A Differential/Algebraic System Solver," SAND--82-8637, Sandia National Laboratories, Montreal, Canada (1982).
27. W. M. STACEY, *Nuclear Reactor Physics*, Wiley-VCH Verlag GmbH & Co. KGaA, Weinheim, Germany (2007); https://doi.org/10.1002/9783527611041.
28. E. M. BAUM et al., *Chart of the Nuclides: Nuclides and Isotopes 17th Edition*, Seventeenth, Bechtel Marine Propulsion Corporation (2009).